

Activated and Metallic Conduction in *p*-Type Modulation-Doped Ge-Sn Devices

Y. Gul^{1,*}, M. Myronov^{2,†}, S.N. Holmes¹, and M. Pepper^{1,3}

¹*London Centre for Nanotechnology, University College London, 17–19 Gordon Street, London WC1H 0AH, United Kingdom*

²*Department of Physics, University of Warwick, Coventry CV4 7AL, United Kingdom*

³*Department of Electronics and Electrical Engineering, University College London, Torringdon Place, London WC1E 7JE, United Kingdom*



(Received 11 June 2020; revised 2 November 2020; accepted 3 November 2020; published 24 November 2020)

$Ge_{1-x}Sn_x$ quantum wells can be incorporated into Si-Ge-based structures with low-carrier effective masses, high mobilities, and the possibility of direct band-gap devices with $x \sim 0.1$. However, the electrical properties of *p*-type $Ge_{1-x}Sn_x$ devices are dominated by a thermally activated mobility and metallic behavior. At 30 mK the transport measurements indicate localization with a mobility of $380 \text{ cm}^2/\text{Vs}$, which is thermally activated with a temperature-independent carrier density of $4 \times 10^{11} \text{ cm}^{-2}$. This weakly disordered system with conductivity, $\sigma \sim e^2/h$, where e is the fundamental charge and h is Planck's constant, is a result of negatively charged "Sn-vacancy" complex states in the barrier layers that act as hole traps. A measured hole effective mass of $0.090 \pm 0.005m_e$ from the Shubnikov-de Haas effect, where m_e is the free electron mass shows that the valence band is heavy hole dominated and is similar to *p*-type Ge with the compressive strain playing the role of quenching the spin-orbit coupling and shifting the unoccupied light-hole states to higher hole energies. The $Ge_{1-x}Sn_x$ devices have a high quantum mobility of approximately $36\,000 \text{ cm}^2/\text{Vs}$ that is *not* thermally activated. The ratio of transport-to-quantum mobility of approximately 0.01 in $Ge_{1-x}Sn_x$ devices is unusual and points to several competing scattering mechanisms in the different experimental regimes.

DOI: [10.1103/PhysRevApplied.14.054064](https://doi.org/10.1103/PhysRevApplied.14.054064)

I. INTRODUCTION

A. General introduction to Ge-Sn

Direct band-gap Ge electronic devices can be achieved by replacing the active Ge layer in a structure with a $Ge_{1-x}Sn_x$ alloy with x from 0 to 1. In practice, low values of x (typically <0.1 [1,2]) are needed for the minimum in the conduction band to switch from being the indirect, L -like to the direct band gap at the Γ point. The direct nature of the band gap means that Ge photonic devices are feasible [3] using Ge-Sn layers for an extension of the Ge device road map into photonic devices [4]. Monolithic integration of optical and electrical devices in Ge have been reviewed recently [5] and this technology is an exciting prospect when Sn alloying is included. An outstanding issue that is addressed in this paper is whether electrical devices in such optically integrated systems would be compatible with low-disorder high-speed quantum devices.

Conventional *p*-channel MOSFET devices have already been fabricated with doped Ge-Sn layers [6,7] and in

Ref. [8] a *p*-MOSFET was reported with a mobility of $509 \text{ cm}^2/\text{Vs}$. These devices were not measured at low temperatures and the problem of disorder in the devices was not considered. The origin of disorder and the influence of this on the conductivity in the Si-based MOSFET was reported in Ref. [9,10]. The present device schemes involve a modulation doping design unlike the Si MOSFET, however the device conductivity is still influenced by disorder. This disorder in the *p*-channel Ge-Sn modulation doped structure is a result of Sn-vacancy defect states in the barriers that act as hole traps and could limit the application of this system into quantum devices.

In this paper we discuss the following details of magnetotransport in Ge-Sn quantum wells. Section I B and I C are further introductions to Ge-Sn. Section II discusses the growth and processing of the wafers and the experimental details. In Sec. III the experimental data on low-temperature transport is presented on four different devices from several cryostat systems from 30 mK to 5 K. Section IV is a discussion of the main points with the conclusions laid out in Sec. IV.

B. Introduction to the valence band in Ge-Sn

The compressive strain in the Ge-Sn grown on relaxed Ge reduces the conduction-band minima at the L point,

*y.gul@ucl.ac.uk

†m.myronov@warwick.ac.uk

offsetting the effect of Sn alloying. The direct gap is the minimum gap at 7% Sn [11] for unstrained layers, increasing to 8.6% Sn with a 0.22% compressive strain. Thin sputtered Ge-Sn layers on Ge were reported earlier as changing to direct band gap for >10% Sn [2]. The valence band of Ge-Sn is only weakly changed with alloying with the valence-band states more influenced by strain than channel composition. The degeneracy of the valence band in Ge-Sn is dependent on the strain with the character of the lowest valence-band states remaining heavy-hole-like with Sn compositions [12] with a compressive strain. With tensile strain the hole ground state can be the light-hole states [13] but this is not the case with epitaxial Ge-Sn layers on relaxed Ge layers.

High transport mobilities are predicted for Ge-Sn [6,14] and embedded Ge-Sn layers can form the channel of a tunneling FET device [15]. The Ge-Sn quantum well (QW) in a Ge structure is under compressive strain and in this case the lowest conduction band is at the L point rather than at the Γ point in this alloy for the unstrained material. The ground state in the valence band is the heavy-hole state (J_z , total angular momentum = 3/2 and m_J , z components of angular momentum = ±3/2) with light in-plane mass. The hole effective mass is very similar to that in p -type strained Ge QWs [16], which is not surprising as the level of strain is similar and the valence-band parameters with a dilute Ge-Sn alloy are not fundamentally different to Ge [14].

C. Introduction to activated conductivity

In two-dimensional systems all states are localized [17], however inelastic scattering processes can cause an activated conductivity at low temperatures between localized states. Initially an effective medium theory [18] is used to explain this but in fact percolation arguments [19] are used to understand how the disordered Si surface inversion layer of two-dimensional charge can conduct with thermal activation to a critical percolation threshold. The original ideas on this effect could not fully explain why a conductivity that is thermally activated with the Fermi energy below the percolation-threshold energy also had constant carrier density and charge carriers are not trapped but contributed to the Hall effect. The metallic behavior observed either as a Shubnikov-de Haas effect or a cyclotron resonance [20] in applied magnetic fields is due to the Fermi energy being above the mobility edge. The conductivity (σ) as a function of temperature (T) is via extended states at the percolation threshold, see Eq. (1),

$$\sigma_{\text{extended}} = \sigma_o e^{-(T_o/T)}, \quad (1)$$

where σ_o is the high-temperature intercept, and T_o is the characteristic temperature. The activation energy to the critical conducting percolation threshold is then $k_B T_o$, where k_B is the Boltzmann constant. At lower carrier densities in the Si inversion layer, an Anderson transition is seen

[10,21] in both n - and p -type channels with the concept of the minimum metallic conductivity postulated earlier [22] playing a role. In this case the transport mechanism is that of Mott variable range hopping (VRH), which in two dimensions is described by Eq. (2) in the conductivity,

$$\sigma_{\text{VRH}} = \sigma_o e^{-(T_M/T)^{1/3}}, \quad (2)$$

where T_M is the nonuniversal, characteristic Mott temperature and is device and carrier density dependent. σ_o is the high-temperature intercept and has a universal value of $2e^2/h$ for Mott VRH, where e is the fundamental charge and h is Planck's constant. In the percolation regime, the mobility ($\mu = \sigma R_H$) is thermally activated where R_H is the Hall constant that is dependent on the nonthermally activated hole density (p) with $p = 1/(eR_H)$. Equation (3) comes from the thermal activation of the conductivity, where the mobility has the same characteristic temperature T_o or thermal-activation energy $k_B T_o$,

$$\mu = \mu_o e^{-(T_o/T)}, \quad (3)$$

In Ref. [23] thermally activated holes were reported in a Si inversion layer. The devices were surface gated to map the change in thermal-activation energy with inversion-layer carrier density and metallic behavior with an activated mobility was observed. An activated mobility was also seen in the two-dimensional electron gas in a Si inversion layer [9,24]. An explanation of this was given in Ref. [25] but this involved a correlation effect of the entire two-dimensional system behaving as a viscous liquid state.

II. FABRICATION OF Ge-Sn DEVICES

A. Growth of wafers

The Ge-based Ge-Sn wafers are grown by reduced-pressure chemical vapor deposition in an *ASM Epsilon* system. The precursor materials are SnCl_4 and Ge_2H_6 with an overall H_2 atmosphere in the growth system. Segregation of Sn is a known problem in structures with Sn > 7% [26,27], although this effect is minimized here by using low growth temperatures, approximately 270 °C. The maximum incorporated Sn concentration is approximately 8% with the present growth conditions and the nonincorporated Sn can surface segregate, although there is no evidence for metallic Sn aggregation [27] on the surface of the wafers measured. Residual Sn atoms that segregate into the Ge cap can find a vacancy and form a defect that is a hole trap approximately 190 meV from the heavy-hole band edge [28]. The influence of Sn-vacancy traps as the main source of disorder on the carrier density and mobility is discussed further in the paper. The 15-nm-thick Ge-Sn QW had an intended composition of 9.3% Sn. This nominal composition is higher than that expected for the growth conditions. SIMS measurements indicate that

there is an accumulation of excess Sn in Ge barrier layer with the composition in the quantum well closer to 8% Sn. The surface roughness of the wafer is $< 2 \text{ nm}$ and there are no metallic Sn dots on the wafer surface. Figure 1(a) shows a cross section of the wafer structure. This wafer doping design is an “inverted-doping” structure, where the modulation doping layer is between the QW and the substrate. This inverted-doping structure usually results in a lower hole mobility compared to the normally doped scheme in Ge-based devices [29] but the potential for gate leakage with Schottky surface gates is reduced significantly in the case of the inverted-doping interface.

The $\text{Ge}_{0.92}\text{Sn}_{0.08}$ QW has compressive strain of approximately 1.3% with respect to the unstrained Ge cladding layers. The strain increases the gap at the Γ point with the L minimum still the lowest part of the conduction band [12,13]. Figure 1(b) shows the self-consistent calculation of the full band structure, calculated using *Nextnano* [30]. The effect of the compressive strain is shown with the degeneracy between the light- and heavy-hole states removed at the top of the valence band in the Ge-Sn QW. Previous optical measurements on similar structures from the same growth system [31] have demonstrated high epitaxial-wafer quality. The devices are *p*-type modulation doped with boron to a doping density of approximately 10^{18} cm^{-3} , see Fig. 1(a). The modulation doping

density is confirmed by SIMS. *In situ* illumination of the devices with a light-emitting diode at low temperatures can increase the carrier density by approximately 10% showing that most of the dopant is activated in this type of heterostructure even in the low-temperature growth regime used here.

B. Device fabrication

Standard Hall bar mesas are fabricated using optical lithography and $\text{HCl}/\text{H}_2\text{O}_2/\text{H}_2\text{O}$ etchant. The Ohmic contacts are formed by sputtering 130 nm of Pt. The contacts are not annealed during the processing; this unusual situation is discussed in Ref. [32], where annealing at low temperatures tended to form resistive Pt_2Ge_3 rather than conductive PtGe_3 interlayers in the Ohmic contact region. This Ohmic contacting scheme is sufficient for Ge-based nanostructures that operate at low temperatures [33,34]. A total of four Hall bar devices are measured, showing consistent transport properties.

C. Experimental details

The measurements reported here are taken in three different cryostats: (i) an 8-T Oxford Instruments variable temperature insert system, (ii) an 8-T Oxford Instruments

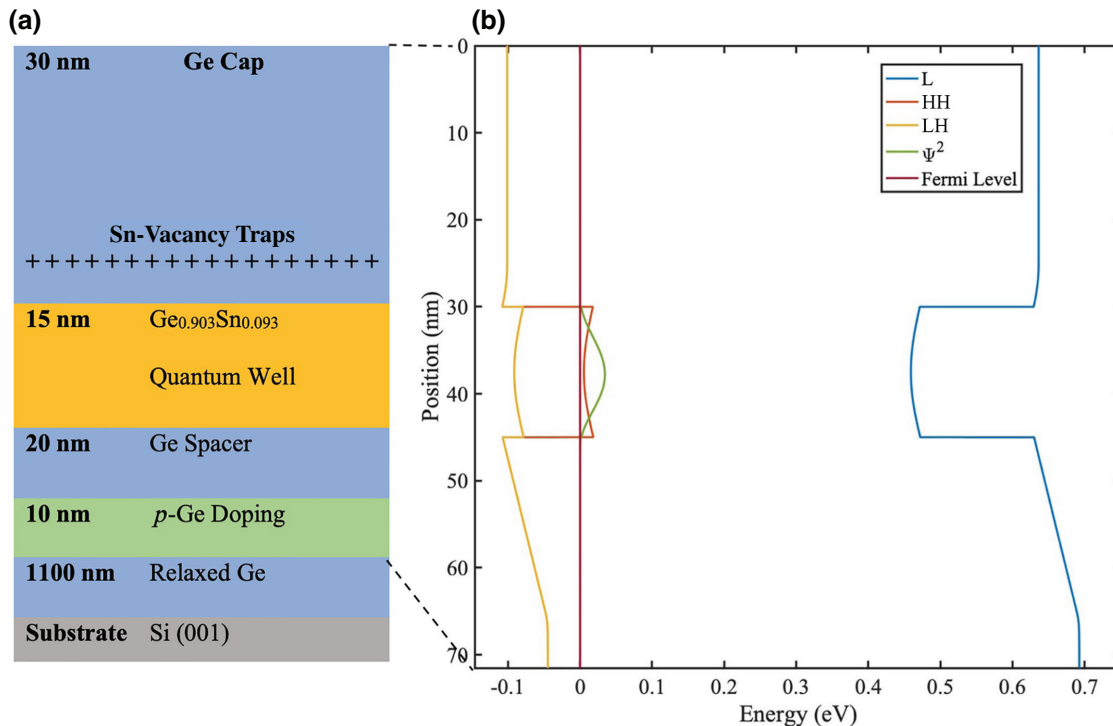


FIG. 1. (a) Schematic of the wafer structure used to fabricate Ge-Sn devices. The thicknesses are not to scale. (b) A band-structure calculation of the strained $\text{Ge}_{0.92}\text{Sn}_{0.08}$ 15-nm QW and surrounding doped layers from the *Nextnano* software [30]. L refers to the lowest conduction band, LH to the light-hole band and HH to the heavy-hole band. The magnitude of the wave function ($|\Psi|^2$) is shown, confined to the Ge-Sn QW.

Teslatron system, and (iii) an Oxford Instruments Triton-2 dilution refrigerator with applied fields of 10 T. The devices are measured in the dark and after *in situ* illumination at low temperatures (T) with the longitudinal resistivity (ρ_{xx}) and Hall resistivity (ρ_{xy}) measured as a function of magnetic field (B) at constant temperature. At temperatures < 1.5 K low excitation currents (< 5 nA) are used at 33 Hz to minimize heating the hole gas above the device lattice temperature set by the temperature of the mixing chamber plate in the dilution fridge.

III. EXPERIMENTAL SECTION

A. Conductance and mobility

Taking the range of mobility values from four different devices, the mean mobility in the dark at 1.5 K is $1080 \text{ cm}^2/\text{Vs}$ with a carrier density of $4.1 \pm 0.1 \times 10^{11} \text{ cm}^{-2}$. After illumination the hole density increases to $4.5 \pm 0.1 \times 10^{11} \text{ cm}^{-2}$ with a reduced mean mobility of $1030 \text{ cm}^2/\text{Vs}$. These mobility values are typical of the low mobility measured in disordered *p*-type Si-Ge alloy QWs [35,36], even with offset modulation doping. Figure 2 shows the low magnetic field transport properties of device 2 from 250 mK to 5 K. Figure 2(a) shows the four terminal conductivity in units of e^2/h . σ is determined from $1/\rho$, where ρ is the measured four-terminal zero-field resistivity. The carrier concentration (p) measured from the Hall effect is $4.16 \times 10^{11} \text{ cm}^{-2}$ and is independent of temperature from 30 mK to 5 K. In Fig. 2(a) σ is plotted as a function of $1/T$ down to 250 mK. At temperatures less than approximately

300 mK the conductivity saturates at $0.68e^2/h$. Although σ is $< e^2/h$ the conduction is by thermal activation to extended states not VRH. Equation (1) fits the experimental data between 2 K and 600 mK. The high-temperature intercept is $2.6e^2/h$, which is too high for a VRH conductance. Figure 2(b) shows the mobility as a function of $1/T$. An Arrhenius thermal activation of μ fits to Eq. (3) with the same characteristic T_o of 0.7 K as the conductivity fit. This activated mobility shows strong evidence for localization of holes in the device below a percolation threshold [23]. The Sn-vacancy trap states in the Ge surface capping layer provides a sheet of negative charges that confine the two-dimensional holes to locally high-density regions of this defect. The thermal activation of the mobility then represents a percolation of charge along the channel. There is no thermal activation of the hole density with the measured carrier density independent of temperature from 30 mK to 5.0 K, which is the highest measurement temperature. The highest transport mobility measured is approximately $1400 \text{ cm}^2/\text{Vs}$ in device 2 at 5.0 K and this is the highest hole mobility reported for modulation-doped Ge-Sn devices. It is already shown that in *p*-Si-Ge the device mobility is reduced significantly below that expected for remote ionized impurity-dominated scattering [35–37]. However, in strained *p*-Ge mobilities of approximately $10^6 \text{ cm}^2/\text{Vs}$ are possible [38,39] with the same modulation doping and doping offset distance of 20 nm. This reduction in mobility in *p*-Ge-Sn devices by approximately 10^3 compared to *p*-Ge and thermal activation is a consequence of the Sn-vacancy hole trap in the Ge cap layer.

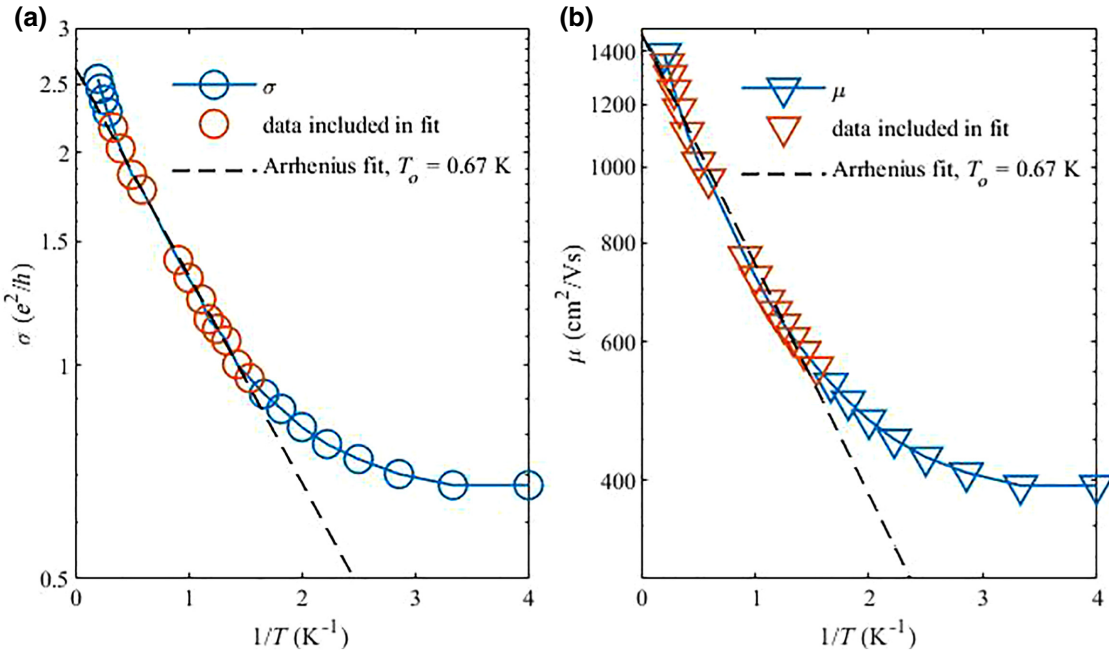


FIG. 2. (a) The conductivity and (b) the mobility as a function of inverse temperature. The fits show thermally activated behavior.

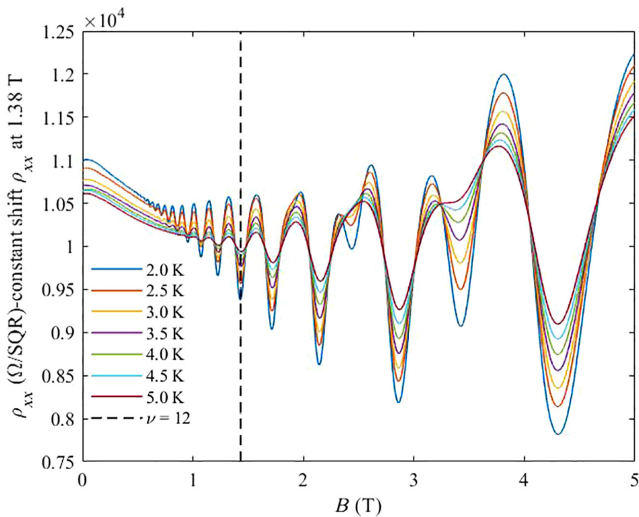


FIG. 3. The temperature dependence of ρ_{xx} up to 5 T and from 2.0 to 5.0 K with a hole density of $4.1 \times 10^{11} \text{ cm}^{-2}$. The curves are offset to align ρ_{xx} at 1.38 T.

B. Transport measurements at 1.5 K

The Shubnikov-de Haas effect in ρ_{xx} for device 2 between 2.0 and 5.0 K is shown in Fig. 3. As a consequence of the large temperature variation in the zero-field resistivity, the individual field sweeps at constant temperature are shifted by a constant offset to align ρ_{xx} at 1.38 T. This corresponds to a filling factor (ν) of 12.5 from the fundamental field (B_f) of approximately 8.54 T. The fundamental field does not vary with temperature and corresponds to a constant hole density of $4.1 \times 10^{11} \text{ cm}^{-2}$. The Hall resistivity data is shown in Fig. 4(a) for the same range of temperatures. The Hall effect hole density is $4.2 \times 10^{11} \text{ cm}^{-2}$ showing good agreement with the Shubnikov-de Haas density and that there is no parallel conduction in the device structure from the surface, doping supply layer, thick Ge buffer layers, or a band of disordered low mobility carriers. The plateaus in the quantum Hall effect are narrow (< 0.3 T width at $\nu = 4$) and are more characteristic of a low-disorder system, comparable to that in strained *p*-Ge, inverted-doping QWs [29].

Figure 4(b) shows the amplitude of the Shubnikov-de Haas effect signal plotted as $\Delta\rho_{xx}/\rho_{xx}$ at $\nu = 12$ (1.423 T) as a function of temperature. The triangles correspond to the experimental data and the solid lines correspond to effective-mass contours of the thermal damping term in the Shubnikov-de Haas amplitude, given by Eq. (4) with effective mass (m^*) values from $0.085m_e$ to $0.100m_e$, with m_e the free electron mass,

$$\Delta\rho_{xx}/\rho_{xx} \sim \frac{X}{\sin hX} \text{ where } X = \frac{2\pi^2 m^* kT}{\hbar e B} \quad (4)$$

and \hbar is the reduced Planck constant. A similar analysis at odd filling factor $\nu = 13$ before the onset of the Zeeman splitting, indicates the same effective-mass value. This analysis assumes that the quantum mobility is not changing significantly with temperature and that $\Delta\rho_{xx}/\rho_{xx} \ll 1$. The Shubnikov-de Haas effect gives a heavy-hole effective mass of $0.090 \pm 0.005m_e$ from amplitude analysis of ρ_{xx} at $\nu = 12$ and $\nu = 13$. Previous measurements of the effective mass in *p*-Ge have determined values of approximately $0.080m_e$ [16], approximately $0.065m_e$ [39], and also by the present authors as approximately $0.10m_e$ in the *p*-type Ge devices reported in Ref. [40]. This similarity is due to the fact that the valence-band parameters are influenced more by the compressive strain rather than dilute alloying of Sn into the Ge band structure. The heavy-hole mass in the out-of-plane [001] direction is calculated to be $0.19m_e$ (at 300 K) using a 30-band *k*-*p* theory [41]. This is not inconsistent with the present device as the in-plane mass is measured here at 1.5 K. The light-hole band is shifted in hole energy above the heavy-hole states by approximately 100 meV (from the *Nextnano* calculations [30]) and is not populated at this carrier density with compressive strain in the QW. This large splitting indicates that any mixing of valence-band states is small.

The spin splitting in the Shubnikov-de Haas is from the Zeeman effect of the heavy hole, $J = 3/2$ states and not from any Rashba spin-orbit coupling in the heavy-hole band [42]. There is no indication of beating in the Shubnikov-de Haas effect oscillations or multiple fundamental fields. The Zeeman effect spin splitting starts at $\nu = 9$ (at approximately 1.9 T), with odd filling-factor plateaus also seen in the quantum Hall effect as expected.

C. Transport measurements at 30 mK

At 30 mK the transport mobility is $380 \text{ cm}^2/\text{Vs}$ in device 2 with carrier density of $4.4 \times 10^{11} \text{ cm}^{-2}$. The carrier density is slightly higher in the Triton-2 fridge compared to the 1.5 K system due to a slower cool down to base temperature and there is no indication that the carrier density is thermally activated at 30 mK. The Shubnikov-de Haas effect can be seen in Fig. 5(a) up to 5 T and the corresponding FFT shows a single fundamental field at 9.1 T, see Fig. 5(b). A second peak at a fundamental field of 18 T in the FFT is a harmonic, which shows there are higher frequencies in the oscillatory structure even before odd minima are visible in ρ_{xx} . The single particle or quantum mobility (μ_q) can be determined from the half width at half height of the FFT peak (δB_f) in Fig. 5(b) and is given by Eq. (5),

$$\mu_q = \frac{\sqrt{3}}{\delta B_f}. \quad (5)$$

A δB_f of 0.46 ± 0.02 T corresponds to $\mu_q = 37700 \pm 2000 \text{ cm}^2/\text{Vs}$. This μ_q value is close to agreement with

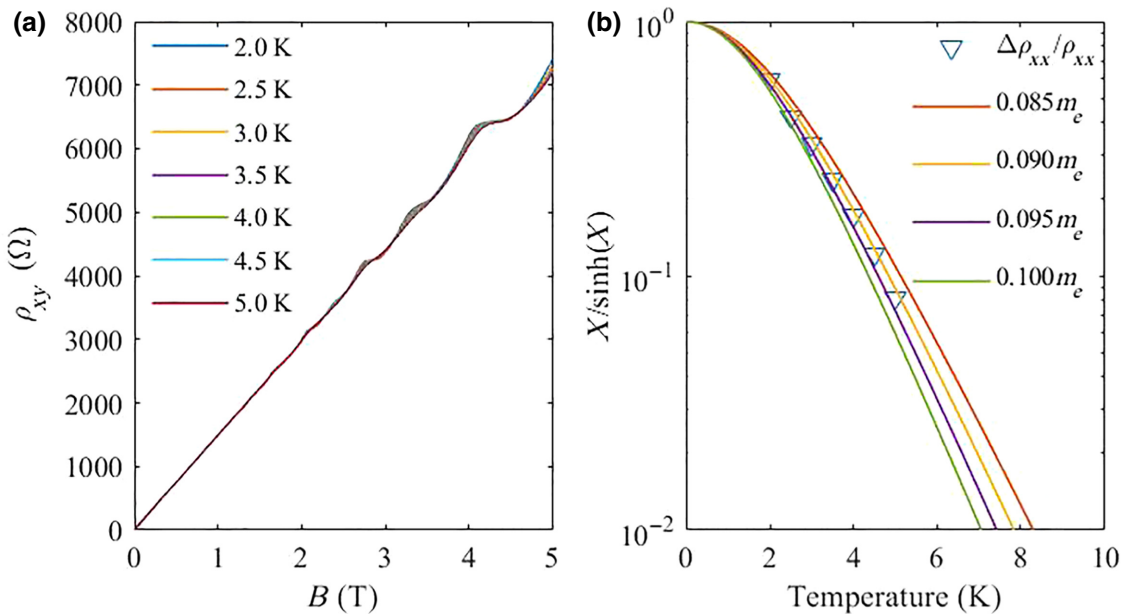


FIG. 4. (a) Quantum Hall effect showing low-disorder plateaus and a constant carrier density, (b) shows the temperature dependence of the amplitude of ρ_{xx} at $\nu = 12$ (1.423 T) from 2.0 to 5.0 K and the thermal damping factor $X/\sinh X$ for effective mass values from 0.085 to $0.100 m_e$. The best fit is at $m^* = 0.090 \pm 0.005 m_e$.

the mobility from the condition of $\mu_q B \approx 1$ at the onset of the Shubnikov-de Haas effect, see Fig. 6. This gives $\mu_q = 34\,000 \text{ cm}^2/\text{Vs}$ with $B = 0.29 \text{ T}$. The quantum mobility determined from analysis of the Shubnikov-de Haas effect, either from the FFT or from the onset of the oscillatory structure is not thermally activated and Eq. (3) does not describe μ_q in $\text{Ge}_{0.92}\text{Sn}_{0.08}$ quantum structures. This also justifies using Eq. (4) to estimate the effective mass from thermal damping of the Shubnikov-de Haas effect amplitude.

Figure 6 shows that at low magnetic field a positive magnetoresistance is seen before the onset of the Shubnikov-de Haas effect. This is also a characteristic of localization in the system although it has disappeared at temperature $> 500 \text{ mK}$ at which point the transport mobility is then thermally activated at higher temperatures, see Fig. 2(b). The positive magnetoresistance at low magnetic field is also characteristic of the magnetoresistance for the inverted-doping structure in p -Ge [29] although in the p -Ge devices this effect does persist to higher than 1.5 K.

IV. DISCUSSION

A. Summary of localization in Ge-Sn

In high-mobility GaAs/(Al,Ga)As two-dimensional systems the ratio (α) of the transport to the quantum mobility can be 10 to 100 [43]. Small angle-scattering events can be correlated and this creates a mobility ratio closer to 1 but still > 1 . An $\alpha \sim 30$ for the inverted-doping interface devices in p -Ge was determined in Ref. [29] and

approximately 18 in Ref. [39]. In the $\text{Ge}_{0.92}\text{Sn}_{0.08}$ QWs measured here $\alpha = 0.011 \pm 0.001$. The situation where the quantum mobility is larger than the transport mobility is unusual and indicates that different scattering mechanisms have to be involved when a large magnetic field is applied to the device. In particular, the quantum mobility is not thermally activated unlike the transport mobility reported in Sec. III A.

The density of scattering centers (N_t) can be estimated from $N_t = 4/(\pi l_e^2)$ where the elastic mean free path, $l_e(\text{nm}) = 1.65 \cdot 10^{-6} \sqrt{\rho} \mu$. The mobility μ (in units of m^2/Vs) is the high-temperature intercept in Fig. 2(b) of $0.15 \text{ m}^2/\text{Vs}$ and the hole density is $4.4 \times 10^{15} \text{ m}^{-2}$, giving an l_e of 16.4 nm. If the scattering rate is fully dominated by the Sn-vacancy charge traps, then $N_t \sim 4 \times 10^{11} \text{ cm}^{-2}$. This is an over estimation and should be considered as an upper limit. Large angle scattering caused by Sn-vacancy trap states in the Ge surface layer is limiting the transport mobility, however there is still influence of the remote ionized impurity scattering from the intentional B dopants in the doping supply layer and alloy scattering in the QW. As the carrier density increases with illumination, the mobility drops as discussed in Sec. III A. This is characteristic of alloy scattering, interface roughness scattering and remote impurity scattering [35]. Charged interface impurities tend to produce a scattering effect that is only weakly dependent on the free carrier density with the mobility *increasing* for higher carrier density. There may be differences in disorder levels on increasing the carrier density with a gate compared to illuminating the device.

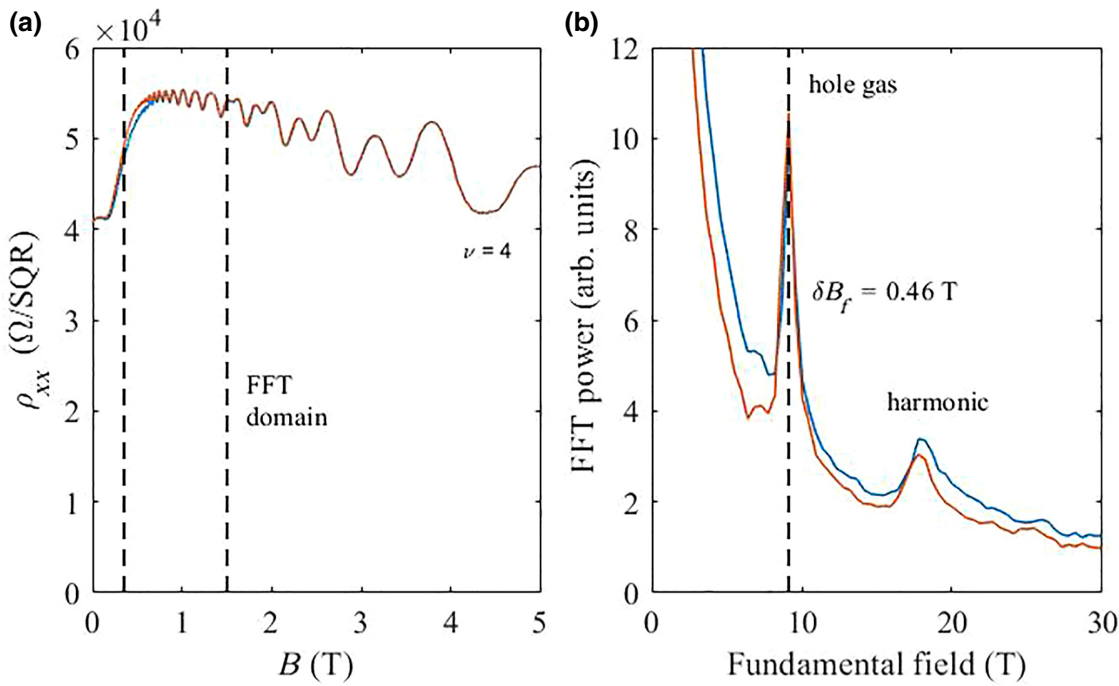


FIG. 5. (a) ρ_{xx} at 30 mK up to 5 T with a carrier density of $4.4 \times 10^{11} \text{ cm}^{-2}$, (b) An FFT from 0.35 to 1.5 T shows a fundamental field of 9.1 T with a quantum mobility (μ_q) of $37\,000 \text{ cm}^2/\text{Vs}$ from the FFT half width at half height (δB_f). Both figures show an up and down field sweep with the vertical scale in (b) in arbitrary units (arb. units), i.e., scaled to 10 at the highest power.

The thermally activated hole mobility is analogous to that in disordered Si *p*-MOSFET devices, although the Arrhenius activation energy is small ($k_B T_o < 0.1 \text{ meV}$) at a hole density of $4.4 \times 10^{11} \text{ cm}^{-2}$. Further top-gating measurements will shift the Fermi energy in depletion closer to the bottom of the valence band where a Mott VRH regime could be established, see Sec. I C. Alternatively a Coulomb gap could be stabilized [36,44] with α closer to approximately 1 as expected for dominant scattering due to (remote) impurities at the Ge-Ge_{0.92}Sn_{0.08} interface rather than the remote impurity scattering from the modulation doping supply layer.

The quantum mobility in Ge_{0.92}Sn_{0.08} QWs is comparable to that in ultrahigh mobility strained *p*-Ge. In those *p*-Ge devices ballistic transport phenomena can be observed in one-dimensional devices [33,45] as well as fractional quantization of the ballistic conductance [34]. The quantum mobility in the Ge_{0.92}Sn_{0.08} QW device is determined by remote ionized acceptor scattering from the modulation doping as in the *p*-Ge system and not by the Sn-vacancy trap states. In the Ge_{0.92}Sn_{0.08} devices a Shubnikov-de Haas oscillation can be seen down to a filling factor of $\nu = 58$, a clear indicator of a high quantum mobility.

B. Impurity band conduction

The heavy-hole effective mass from the thermal damping of the Shubnikov-de Haas effect is $0.090 \pm 0.005 m_e$

as determined in Sec. III B. An estimation of the two-dimensional density of states using this mass value gives $3.7 \pm 0.2 \cdot 10^{10} \text{ cm}^{-2} \text{ meV}^{-1}$ and a corresponding Fermi energy of $10.7 \pm 0.7 \text{ meV}$ for a hole density of 4

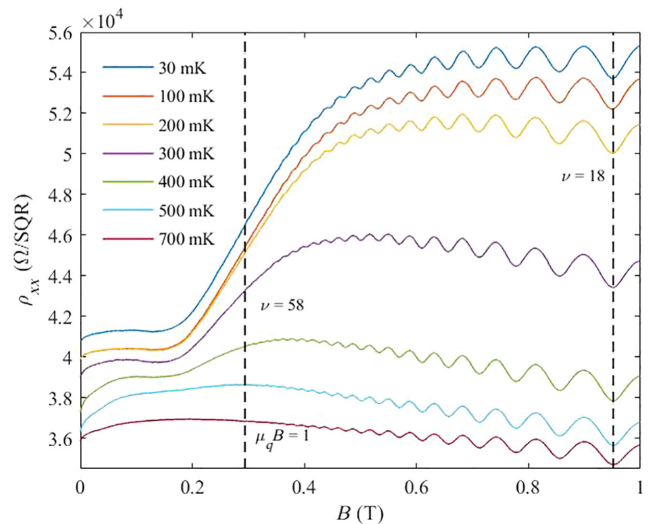


FIG. 6. ρ_{xx} up to 1 T from 30 to 700 mK. The oscillatory structure in ρ_{xx} can be seen down to $\nu = 58$ where the condition $\mu_q B = 1$ is then satisfied. The data for each temperature is plotted on the same scale, however the data for temperatures between 100 and 700 mK is shifted vertically by an arbitrary resistivity.

10^{11} cm $^{-2}$. The hole density is not thermally activated and does not correspond to transport in an impurity band of boron dopant close to the valence-band edge. Even if an impurity band associated with the upper Hubbard state was present from positively charged acceptor states in the boron modulation doping, not the Sn-vacancy traps, this is approximately 1 meV below the valence-band edge [46] and is unlikely to be operating in this system due to the approximately 10.7 meV Fermi energy with the conductivity not being described by hopping transport through these states. The triplet state of the upper Hubbard band can be on the order of meV above the valence-band edge but below the mobility edge and this is unlikely to be playing a role in the transport of the Ge_{0.92}Sn_{0.08} QWs.

V. CONCLUSIONS

The coexistence of localization and metallic behavior of heavy holes in the Ge_{0.92}Sn_{0.08} QW valence band is presented. The measured low-temperature quantum mobility of 36 000 cm 2 /Vs is comparable to that in strained *p*-type Ge QWs that have transport mobilities in the region of 10 6 cm 2 /Vs. However, in Ge_{0.92}Sn_{0.08} a low transport mobility of 380 cm 2 /Vs is a result of the disorder caused by Sn segregation in the growth of the structure into the surface Ge layer as confirmed by SIMS measurements. The Sn then forms a hole trap with a lattice vacancy complex in the Ge barrier layer close to the QW. The conductivity and transport mobility are thermally activated and show Arrhenius behavior with a temperature-independent hole density, similar to the Si-MOSFET device with excess charge traps in the surface oxide layer.

The ratio of transport mobility to quantum mobility is 0.011 ± 0.001 , strongly indicating that different scattering mechanisms are at play in the two transport regimes. In applied magnetic fields, the mobility is limited by scattering with remote ionized impurities, analogous to the case of ultrahigh mobility modulation doped *p*-Ge. However, the transport mobility at zero field is a result of scattering with the Sn-vacancy traps in the Ge surface layer.

There is potential for transport devices in Ge-Sn QWs considering the high quantum mobility reported in this publication. With growth optimization, the Sn-segregation problem can be reduced and the prospect of alternative quantum functionality integrated with monolithic optical devices in a Si-based system is appealing. The Ge-Sn QW devices can also be *n*-type doped offering complementary-based electronic devices. The modulation-doped Ge-Sn structure with controllable disorder offers devices for elucidating the metal-insulator transition in the realm of many-body localization [47] with the requisite thermal isolation easily achievable between the Ge-Sn channel layer and the Si substrate using conventional lithography.

ACKNOWLEDGMENTS

This work is supported by the EPSRC at Warwick and at UCL Grant No. EP/R029075/1.

- [1] E. Kasper, J. Werner, M. Oehme, S. Escoubas, N. Burle, and J. Schulze, Growth of silicon based germanium tin alloys, *Thin Solid Films* **520**, 3195 (2012).
- [2] H. Perez Ladron de Guevara, A. G. Rodriguez, H. Navarro-Contreras, and M. A. Vidal, Determination of the optical energy gap of Ge_{1-x}Sn_x alloys with $0 < x < 0.14$, *Appl. Phys. Lett.* **84**, 4532 (2004).
- [3] M. Oehme, J. Werner, M. Gollhofer, M. Schmid, M. Kaschel, E. Kasper, and J. Schulze, Room-temperature electroluminescence from GeSn light-emitting pin diodes on silicon, *IEEE Photonics Tech. Lett.* **23**, 1751 (2011).
- [4] S. Gupta, R. Chen, B. Magyari-Kope, Hai Lin, A. Nainani, Y. Nishi, J. S. Harris, and K. C. Saraswat, in *IEDM Conference IEEE* (2011).
- [5] Shinichi Saito, Abdelrahman Zaher Al-Attili, Katsuya Oda, and Yasuhiko Ishikawa, Towards monolithic integration of germanium light sources on silicon chips, *Semicond. Sci. Technol.* **31**, 043002 (2016).
- [6] Genquan Han, Shaojian Su, Yue Yang, Pengfei Guo, Xiao Gong, Lanxiang Wang, Wei Wang, Cheng Guo, Guangze Zhang, Chunlai Xue, Buwen Cheng, and Yee Chia Yeo, High hole mobility in strained germanium-tin (GeSn) channel pMOSFET fabricated on (111) substrate, *ECS Trans.* **50**, 943 (2012).
- [7] Suyog Gupta, Yi-Chiau Huang, Yihwan Kim, Errol Sanchez, and Krishna C. Saraswat, Hole mobility enhancement in compressively strained Ge_{0.93}Sn_{0.07} pMOSFETs, *IEEE Electr. Dev. Lett.* **34**, 831 (2013).
- [8] Lanxiang Wang, Shaojian Su, Wei Wang, Xiao Gong, Yue Yang, Pengfei Guo, Guangze Zhang, Chunlai Xue, Buwen Cheng, Genquan Han, and Yee-Chia Yeo, Strained germanium-tin (GeSn) p-channel metal-oxide-semiconductor field-effect-transistors (p-MOSFETs) with ammonium sulphide passivation, *Solid-State Electron.* **83**, 66 (2013).
- [9] F. F. Fang and A. B. Fowler, Transport properties of electrons in inverted silicon surfaces, *Phys. Rev.* **169**, 619 (1968).
- [10] M. Pepper, S. Pollitt, and C. J. Adkins, Anderson localisation of holes in a Si inversion layer, *Phys. Lett. A* **48**, 113 (1974).
- [11] Robert Chen, Hai Lin, Yijie Huo, Charles Hitzman, Theodore I. Kamins, and James S. Harris, Increased photoluminescence of strain-reduced, high-Sn composition Ge_{1-x}Sn_x alloys grown by molecular beam epitaxy, *Appl. Phys. Lett.* **99**, 181125 (2011).
- [12] Z. Xiao, N. Goldsman, and N. K. Dhar, Effects of volumetric and potential energy change on indirect to direct bandgap transition of Ge/Sn alloy, *J. Appl. Phys.* **125**, 135705 (2019).
- [13] Robert Chen, Suyog Gupta, Yi-Chiau Huang, Yi jie Huo, Charles W. Rudy, Errol Sanchez, Yihwan Kim, Theodore I. Kamins, Krishna C. Saraswat, and James S. Harris, Demonstration of a Ge/GeSn/Ge quantum-well microdisk resonator on silicon: Enabling high-quality

- Ge(Sn) materials for micro- and nanophotonics, *Nano Lett.* **14**, 37 (2014).
- [14] Jay Deep Sau and Marvin L. Cohen, Possibility of increased mobility in Ge-Sn alloy system, *Phys. Rev. B* **75**, 045208 (2007).
- [15] S. Wirths, A. T. Tiedemann, Z. Ikonic, P. Harrison, B. Holländer, T. Stoica, G. Mussler, M. Myronov, J. M. Hartmann, D. Grützmacher, D. Buca, and S. Mantl, Band engineering and growth of tensile strained Ge/(Si)GeSn heterostructures for field effect transistors, *Appl. Phys. Lett.* **102**, 192103 (2013).
- [16] B. Rössner, G. Isella, and H. von Känel, Effective mass in remotely doped Ge quantum wells, *Appl. Phys. Lett.* **82**, 754 (2003).
- [17] E. Abrahams, P. W. Anderson, D. C. Licciardello, and T. V. Ramakrishnan, Scaling Theory of Localization: Absence of Quantum Diffusion in Two Dimensions, *Phys. Rev. Lett.* **42**, 673 (1979).
- [18] Uzi Even and Joshua Jortner, Experimental relations for the hall effect near the metal insulator transition, *Phil. Mag.* **25**, 715 (1972).
- [19] Richard Zallen and Harvey Scher, Percolation on a continuum and the localization-delocalization transition in amorphous semiconductors, *Phys. Rev. B* **4**, 4471 (1971).
- [20] D. C. Tsui and S. J. Allen Jr., Mott-Anderson Localization in the Two-Dimensional Band Tail of Si Inversion Layers, *Phys. Rev. Lett.* **32**, 1200 (1974).
- [21] M. Pepper, S. Pollitt, C. J. Adkins, and R. E. Oakley, Variable-range hopping in a silicon inversion layer, *Phys. Lett. A* **47**, 71 (1974).
- [22] N. F. Mott, Conduction in glasses containing transition metal ions, *J. Non-Cryst. Solids* **1**, 1 (1968).
- [23] Emil Arnold, Disorder-induced carrier localization in silicon surface inversion layers, *Appl. Phys. Lett.* **25**, 705 (1974).
- [24] J. P. Thompson, Hall effect measurements on silicon inversion layers, *Phys. Lett.* **66A**, 65 (1978).
- [25] C. J. Adkins, Threshold conduction in inversion layers, *J. Phys. C* **11**, 851 (1978).
- [26] Fabio Pezzoli, Anna Giorgioni, David Patchett, and Maksym Myronov, Temperature-Dependent photoluminescence characteristics of GeSn epitaxial layers, *ACS Photonics* **3**, 2004 (2016).
- [27] David Weissaupt, Pedram Jahandar, Gerard Colston, Phil Allred, Jorg Schulze, and Maksym Myronov, Impact of Sn segregation on $\text{Ge}_{1-x}\text{Sn}_x$ epi-layers growth by RP-CVD, MIPRO, Opatija Croatia, 22-26 May p43 (2017).
- [28] V. P. Markevich, A. R. Peaker, B. Hamilton, V. V. Litvinov, Yu. M. Pokotilo, S. B. Lastovskii, J. Coutinho, A. Carvalho, M. J. Rayson, and P. R. Briddon, Tin-vacancy complex in germanium, *J. Appl. Phys.* **109**, 083705 (2011).
- [29] O. A. Mironov, A. H. A. Hassan, M. Uhlarz, S. Kiatgamchai, A. Dobbie, R. J. H. Morris, S. Gabani, I. B. Berkutov, and D. R. Leadley, New RP-CVD grown ultra-high performance selectively B-doped pure-Ge 20nm QWs on (100)Si as basis material for post-Si CMOS technology, *Physica Status Solidi C* **11**, 61 (2014).
- [30] nextnano³ software, <https://www.nextnano.de/nextnano3/>
- [31] S. De Cesari, A. Balocchi, E. Vitiello, P. Jahandar, E. Grilli, T. Amand, X. Marie, M. Myronov, and F. Pezzoli, Spin-coherent dynamics and carrier lifetime in strained $\text{Ge}_{1-x}\text{Sn}_x$ semiconductors on silicon, *Phys. Rev. B* **99**, 035202 (2019).
- [32] V. Janardhanam, Jin-Sung kim, Kyungwon Moon, Young-Boo Lee, Do-Geun Kim, Seung-Min Kang, and Chel-Jong Choi, Electrical and microstructural properties of Pt-germanides formed on p-type Ge substrate, *J. Elect. Chem. Soc.* **158**, H846 (2011).
- [33] Y. Gul, S. N. Holmes, P. J. Newton, D. J. P. Ellis, C. Morrison, M. Pepper, C. H. W. Barnes, and M. Myronov, Quantum ballistic transport in strained epitaxial germanium, *Appl. Phys. Lett.* **111**, 233512 (2017).
- [34] Y. Gul, S. N. Holmes, M. Myronov, S. Kumar, and M. Pepper, Self-organised fractional quantisation in a hole quantum wire, *J. Phys.: Condens. Matter.* **30**, 09LT01 (2018).
- [35] C. J. Emeleus, T. E. Whall, D. W. Smith, R. A. Kubiak, E. H. C. Parker, and M. J. Kearney, Scattering mechanisms affecting hole transport in remote-doped Si/SiGe heterostructures, *J. Appl. Phys.* **73**, 3852 (1993).
- [36] J. Lam, M. D'Iorio, D. Brown, and H. Lafontaine, Scaling and the metal-insulator transition in Si/SiGe quantum wells, *Phys. Rev. B* **56**, R12742 (1997).
- [37] P. T. Coleridge, R. L. Williams, Y. Feng, and P. Zawadzki, Metal-insulator transition at B=0 in p-type SiGe, *Phys. Rev. B* **56**, R12764 (1997).
- [38] A. Dobbie, M. Myronov, R. J. H. Morris, A. H. A. Hassan, M. J. Prest, V. A. Shah, E. H. C. Parker, T. E. Whall, and D. R. Leadley, Ultra-high mobility exceeding one million in a strained germanium quantum well, *Appl. Phys. Lett.* **101**, 172108 (2012).
- [39] C. Morrison, C. Castelaro, D. R. Leadley, and M. Myronov, Complex quantum transport in a modulation doped strained Ge quantum well heterostructures with a high mobility 2D hole gas, *Appl. Phys. Lett.* **109**, 102103 (2016).
- [40] P. J. Newton, J. Llandro, R. Mansell, S. N. Holmes, C. Morrison, J. Feronda, M. Myronov, D. R. Leadley, and C. H. W. Barnes, Magnetotransport in p-type Ge quantum well narrow wire arrays, *Appl. Phys. Lett.* **106**, 172012 (2015).
- [41] Zhigang Song, Weijun Fan, Chuanseng Tan, Qijie Wang, Donguk Nam, Daohua Zhang, and Greg Sun, Band structure of $\text{Ge}_{1-x}\text{Sn}_x$ alloy: A full-zone 30-band $k\cdot p$ model, *New J. Phys.* **21**, 073037 (2019).
- [42] S. N. Holmes, P. J. Newton, J. Llandro, R. Mansell, C. H. W. Barnes, C. Morrison, and M. Myronov, Spin-splitting in p-type Ge devices, *J. Appl. Phys.* **120**, 085702 (2016).
- [43] P. T. Coleridge, Small-angle scattering in two-dimensional electron gases, *Phys. Rev. B* **44**, 3793 (1991).
- [44] A. L. Efros and B. I. Shklovskii, Coulomb gap and low temperature conductivity of disordered systems, *J. Phys. C* **8**, L49 (1975).
- [45] R. Mizokuchi, R. Maurand, F. Vigneau, M. Myronov, and S. Franceschi, Ballistic one-dimensional holes with strong g-factor anisotropy in germanium, *Nano Lett.* **18**, 4861 (2018).
- [46] P. Gross and K. Lassmann, Investigation of positively charged acceptor states in Ge and Si under uniaxial stress by phonon induced conduction, *Ann. Physik* **4**, 503 (1995).
- [47] D. M. Basko, I. L. Aleiner, and B. L. Altshuler, Metal-insulator transition in a weakly interacting many-electron system with localized single-particle states, *Annals Phys.* **321**, 1126 (2006).